Vol. 19, No. 2 (2020) 997-1010
Revista Mexicana de Ingeniería Química

# Improving platinum dispersion on SBA-15 by titania addition

# Mejoramiento de la dispersión de platino soportado sobre SBA-15 por adición de titania

G. Morales-Hernández[1], J.G. Pacheco-Sosa[1], J. Escobar-Aguilar[2*], J.G. Torres Torres[1], H. Pérez-Vidal[1], M.A. Lunagómez-Rocha[1], D. De la Cruz-Romero[1], P. del Ángel-Vicente[2]

[1]*División Académica de Ciencias Básicas (DACB), Universidad Juárez Autónoma de Tabasco (UJAT), Km.1 Carretera Cunduacán-Jalpa de Méndez, Col. La Esmeralda, Cunduacán, Tabasco, México.*
[2]*Instituto Mexicano del Petróleo, Eje Central L. Cárdenas Norte 152, San Bartolo Atepehuacan, G. A. Madero, Cd. de México, México, 07730.*

Received: September 9, 2019; Accepted: November 6, 2019

## Abstract

Pt (1 and 1.5 wt%) was impregnated on SBA-15 and corresponding Ti-modified composites at different $TiO_2$ contents (3, 5, 10 and 20 wt%). Materials were characterized by $N_2$ physisorption, X-ray diffraction, Fourier transformed infrared spectroscopy, scanning electron microscopy and transmission electron microscopy. SBA-15 had surface area greater than 800 $m^2/g$ that decreased with increasing $TiO_2$ content in binary materials. Very different hydrolysis rate of Ti and Si alkoxides could provoke encapsulation of segregated titania domains in SBA-15 structure. Highly reactive titanium butoxide hydrolysis-condensation could occur before reactions corresponding to tetraethyl orthosilicate. Pt dispersion augmented with Ti concentration where numerous tiny metallic particles were observed on titania surface. Also, corresponding pore size maxima shifted to lower diameters (as to that of non-impregnated supports) after platinum loading suggested metallic crystals inside pores of SBA-15 and Ti-modified carriers, that effect being much clearer in the latter. However, large cubic platinum crystals were also observed suggesting sintering (during calcining at 500 °C) of metallic particles weakly interacting with SBA-15. After materials annealing metallic platinum was evidenced (by XRD) pointing out to contribution of organic remains (from Ti and Si alkoxides, ascertained by FTIR) decomposition on noble metal reduction.

*Keywords*: SBA-15, $TiO_2$, platinum, composites, dispersion.

## Resumen

Pt (1 y 1.5 wt%) se impregnó sobre SBA-15 y compósitos con $TiO_2$ (3, 5, 10 y 20%). Materiales se caracterizaron por fisisorción de $N_2$, difracción de rayos X, espectroscopia infrarroja (transformada de Fourier) y microscopía electrónica (barrido y transmisión). SBA-15 presentó área específica superior a 800 $m^2/g$ que disminuyó progresivamente al aumentar $TiO_2$ en soportes mixtos. Diferencia en velocidad de hidrólisis de alcóxidos de Ti y Si pudo provocar encapsulamiento de dominios de titania en SBA-15. Alta reactividad de butóxido de titanio pudo permitir hidrólisis-condensación antes de reacciones del tetraetil ortosilicato. Dispersión de Pt aumentó con concentración de Ti en compósitos observándose numerosas nanopartículas sobre dominios de titania. Asimismo, máximo de distribución porosa de sólidos con platino claramente se desplazó a menores diámetros (respecto a soportes binarios) sugiriendo cristales de Pt en poros de matrices modificadas con Ti. Sin embargo, también se observaron partículas cristales de platino de gran tamaño probablemente debido a sinterizado (durante calcinación a 500 °C) de partículas originalmente depositadas en baja interacción sobre SBA-15. Luego de calcinación (500 °C, aire) Pt metálico fue evidenciado (por DRX) sugiriendo contribución de descomposición de residuos de alcóxidos (identificados por FTIR) en reducción del metal.

*Palabras clave*: SBA-15, $TiO_2$, platino, compósitos, dispersión.

## 1 Introduction

Siliceous mesoporous materials have received much attention due to their multiple potential applications in adsorption and catalysis. The mesoporous molecular sieve SBA-15 (Santa Barbara Amorphous) exhibits interesting characteristics as high surface area (600-1000 $m^2/g$), thick walls (3-6 nm) and significant hydrothermal stability. In addition, Pluronic P123 structure-directing surfactant used during its synthesis (Flodström and Alfredsson, 2003) is cheap, biodegradable and non-toxic (Singh *et al.*, 2018).

* *Corresponding author. E-mail*: jeaguila@imp.mx
https://doi.org/10.24275/rmiq/Mat821
*issn-e*: 2395-8472

That type of siliceous structured solid has been studied as catalysts support due to its uniform mesoporous network that could facilitate interaction of deposited active phases with bulky molecules to be transformed. However, as that of any other $SiO_2$-based matrix SBA-15 surface itself is not particularly adequate to disperse deposited active phases mainly due to its inertness and very low acidity. Thus, a considerable number of efforts have been focused in functionalizing that rather inert siliceous surface. SBA-15 could be efficient nanoreactors where chiral ligands could be incorporated within the cavities of silica matrix being then used to immobilize Pd-species. Those chiral catalysts/ligands within SBA-15 structure could catalyze asymmetric reactions with high enantio and diastereoselectivity (Ziarani *et al*., 2018). As functionalization with the organics and grafting of the metal centers could take place inside the mesoporous framework, catalytic performance could improve proportionally to accesibility to porous network and to surface exposure of substrates to active centers. Expectedly, SBA-15 pore size and volume could significantly influence final catalytic performance.

One interesting approach consists in introducing diverse inorganic heteroatoms (Al, Fe, Ti, etc.) in order to tailor surface properties to specific applications (Zhang *et al*., 2019). In this context, Ti-modified SBA-15 matrices have attracted lots of attention due to their excellent acid properties and mechanical and chemical resistance as well, much superior as to those of other siliceous mesostructured solids (Iglesias *et al*., 2008). For instance, those materials has been studied in glycerol transesterification with dimethyl carbonate to glycerol carbonate (Devi *et al*., 2018). They have also been efficiently applied in high-quality biodiesel production from unrefined canola oil (Sharma *et al*., 2014) and in phenol photocalytic decomposition in liquid phase (Wang *et al*., 2007). However, special attention must be focused in methods used for Ti incorporation into SBA-15 matrices as that could strongly influence textural, structural and surface properties of final binary solids. Titanium content could also play a preponderant rol on mentioned characteristics.

Mesostructured siliceous matrix functionalized by Ti addition have been applied in several reaction schemes. For instance, their use as carrier of NiMoW formulations tested in dibenzothiophene hydrodesulfurization has been reported (Gómez-Orozco *et al*., 2018) where titanium incorporation method used significantly affected morphology, structure and catalytic activity of supported sulfided phases. Also, those binary oxides had been studied as noble metal catalysts supports finding very interesting results. For instance, Pt supported on Ti-modified SBA-15 has been used in CO oxidation (Wu *et al*., 2015), toluene hydrogenation and propane dehydrogenation among other reactions (Zhu *et al*., 2013). However, Pt dispersion on those composites is clearly dependant upon the methodologies used for incorporation of both Pt and titanium in the siliceous matrix (Kolev *et al*., 2014). For instance, for samples at 0.25 wt% Pt supported on SBA-15 modified by 10 wt% Ti it has been reported (Kolev *et al*., 2014) that Ti and Si alkoxides simultaneously added during mixed solids preparation could render binary materials where supported noble metal particle size could be one order of magnitude smaller (4 versus 40 nm) as to that of similar solids where Pt was impregnated on mixed solids prepared by siliceous matrix modification through Ti isopropoxide impregnation. Thus, the search of more efficient methodologies to carry out modifiers incorporation in SBA-15 matrices is presently subject of numerous investigations. It is worh mentioning that improvement of supported Pt-based catalysts results of particular interest as they could be applied in numerous reaction schemes (Torres-Santillán *et al*., 2019; Ballesteros-Plata *et al*., 2019).

In this work, Ti-modified SBA-15 matrices at various $TiO_2$ loadings (3, 5, 10 and 20 wt%) were prepared by directly adding titanium butoxide during TEOS-based SBA-15 synthesis. Pt was deposited (1 and 1.5 wt%) by pore-filling impregnation on obtained composites to assess the effect of titania addition on platinum dispersion. Materials were characterized through several physicochemical instrumental techniques to elucidate their textural, structural and surface properties.

## 2 Materials and methods

### 2.1 Material synthesis

#### 2.1.1 Ti-modified SBA-15

SBA-15 mesoporous materials were synthesized following a well-known preparation protocol (Flodström and Alfredsson, 2003). Thus, triblock copolymer Pluronic P123 ($OE_{20}OP_{70}OE_{20}$ non-ionic surfactant, Sigma-Aldrich, 98 wt%, 19.2 g) was diluted in 450 ml of water and 300 ml of $HNO_3$

(0.5 M, Meyer, 70 wt%) solution were further added. The transparent mixture was kept under vigorous stirring for 24 h at 35 °C. Tetraethyl orthosilicate (TEOS, Sigma-Aldrich, 98 wt%, 40 ml) was used as Si source. After TEOS addition the obtained sol was kept under stirring (600 rpm, ~62 rad/s) for 24 h. Then, the sol was submitted to hydrothermal treatment at 80 °C for 72 h. The obtained gel was filtered, washed with distillated water and dried at room temperature. In order to prepare Ti-modified samples titanium butoxide (TiB, Sigma-Aldrich, 97%) was simultaneously added with TEOS. The amount of TiB utilized corresponded to various $TiO_2$ contents (3, 5, 10 and 20 wt%) in binary composites. All solids were finally calcined at 500 °C for 6 h (2 °C/min heating rate) to obtain mixed oxide composites. Various prepared materials were identified by Ti(x)-SBA-15 key where x stands for $TiO_2$ wt% in composites.

#### *2.1.2 Pt impregnation*

Pt (1.0 and 1.5 wt%) was deposited over SBA-15 and corresponding Ti-modified composites by pore-filling impregnation using chloroplatinic acid ($H_2PtCl_6$ hydrate, Aldrich, 99.9 wt%) as precursor salt. Impregnated solids were left aging for 24 h at room temperature to allow Pt ions diffusion through composites porous network. Materials were further annealed at 500 °C (6 h, 2 °C/min heating rate). As incipient wetness method was used during noble metal salt precursor impregnation we considered that totality of Pt was effectively deposited on carriers. Then, platinum loading refers to nominal values. Various prepared materials were identified by Pt(y)/Ti(x)-SBA-15 key where y stands for impregnated Pt wt% on composites.

#### *2.1.3 Materials characterization*

Textural properties of various prepared materials were determined by $N_2$ physisorption (-198 °C) by using a Micromeritics Tristar II 3020 equipment. Studied solids were previosuly degassed during 4 h (300 °C) to eliminate adsorbed species. Surface area and pore size distribution (PSD) of various studied solids were determined by BET (Brunauer-Emmett-Teller) and BJH (Barret-Joyner-Halenda, desorption data branch) methods, respectively. Samples structural order was studied by powder X-ray difracction utilizing a Bruker D8-Advance diffractometer (CuK$\alpha$ radiation, $\lambda$= 1.5418 Å) at 35 kV accelerating voltage, 25 mA and 0.020° steps. Samples were analyzed by Fourier transformed infrared spectroscopy (FTIR) with a Shimadzu IRAffinity-1 apparatus in the 340-4000 1/cm range at 2 1/cm resolution and 40 scans. Acquired data were processed by using IRsolutionTM software. Wafers were prepared by mixing samples (at 5 wt%) to be studied with KBr (Sigma Aldrich, FTIR grade). Particles morphology was observed by scanning electron microscopy (SEM) in JEOL JSM-6010LA apparatus at 20 kV accelerating voltaje, high vacuum and at various magnifications. Obtained micrographs were processed by using InTouchScope$^{TM}$ software. Materials were characterized by high-resolution transmission electron microscopy (HR-TEM) studies performed in a Titan 80-300 microscope with a Schottky-type field emission gun operating at 300 kV. The point resolution and the information limit were better than 0.085 nm. HR-TEM digital images were obtained using a CCD camera and Digital Micrograph Software from GATAN$^{TM}$. High angle annular dark field in scanning transmission electron microscopy (HAADF-STEM) was performed in the same instrument. In order to prepare the materials for observation, the powdered samples were ultrasonically dispersed in ethanol and supported on lacey carbon coated copper grids.

## 3 Results and discussion

### *3.1 Materials textural properties*

SBA-15 and corresponding Ti-modified solids had type IV $N_2$ adsorption isotherms (Figure 1(a)) with H1 hysteresis as defined by the International Union of Pure and Applied Chemistry (IUPAC) (Sing *et al*., 1985) those isotherm profiles being typical of mesostructured matrices containing cylindrical pores of uniform section (Leofanti *et al*., 1998). Hysthereses loops shape was progressively modified to $H_2$-type probably by influence of titania segregated domains (Cui *et al*., 2019). Textural characteristics of various prepared solids (mixed supports and corresponding Pt-impregnated materials) are shown in Tables 1 and 2. Pristine mesoporous SBA-15 had typical texture with 818 $m^2/g$ surface area ($S_{BET}$), pore volume ($V_p$) of 1.05 $cm^3/g$ and average pore diameter (from corresponding PSD, Figure 1(b)) of 5.78 nm. Those properties nicely corresponded to expected values for SBA-15 matrices (500< $S_{BET}$ >1300 $m^2/g$, 0.82< $V_p$ >1.69 $cm^3/g$) commonly reported in the literature for such type of mesostructured $SiO_2$ (Devi *et al*., 2018;

Schwanke *et al*., 2018).

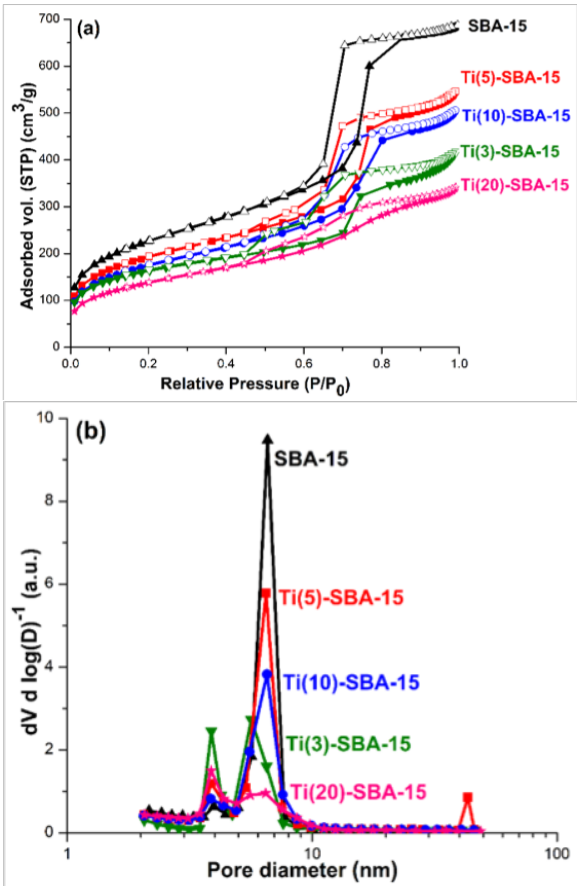


Fig. 1. (a) $N_2$ adsorption isotherms (at -198 °C) of pristine SBA-15 and corresponding Ti-modified materials at various titanium contents. Open symbols: desorption branch; (b) Pore size distribution (BJH) of studied solids.

However, all Ti-modified solids at various contents had decreased surface area as to that of pristine SBA-15. Fifth column of Table 1 shows theoretical surface area of composites considering incorporation of essentially non-porous $TiO_2$ component in SBA-15 matrix ($^bS_{BET}$). Sixth column shows actual $S_{BET}$ of various materials divided over corresponding theoretical ones where textural losses due to non-well dispersed titania phases could be evidenced. Thus, observed values strongly suggested that titania domains could be either partially clogging or disrupting mesoporous siliceous network. Conversely, gradual increase in BET surface area has been reported (Araujo *et al*., 2016) when Ti has been integrated (in tetrahedral coordination) in the silica matrix that effect being attributed to enhanced wall thickness of mixed solid. Corresponding PSD plots of Ti-modified solids (Figure 1(b)) showed contributions related to smaller pores (~3.89 nm) to those of parent SBA-15 pointing out to contributions from $TiO_2$ domains (Araujo *et al*., 2016) suggesting rapid precipitation of titanium hydroxides (from alkoxide hydrolysis, Calzada *et al*., 2019) in aqueous medium at low pH during SBA-15 synthesis (Kolev *et al*., 2014). Neverthelss, presence of some titania domains inside SBA-15 porous network that could provoke shifts to lower diameters in corresponding PSD profiles could not be ruled out (Calzada *et al*., 2019)). After Pt loading on SBA-15 surface area and pore volume importantly diminished (~25%, Table 2). As those losses were much higher than expected considering deposition of non-porous phases that could indicate low platinum dispersion that provoked partial pore plugging of siliceous networks. In this line, it has been reported (Kumar *et al*., 2008) that Pt impregnation (1.3 wt%) by pore filling on SBA-15 could render supported solids of rather large particle size (~21 nm) provoking significantly decreased texture by occluded porosity. However, the lower closing partial pressure of hysteresis loops as to that of corresponding carriers (Figure 2(a)) evidenced that some platinum nanoparticles could be located in interchannels of SBA-15-based supports (Yin *et al*., 2017).

Table 1. Textural properties of SBA-15 and various Ti-SBA-15 materials prepared.

| Sample | $S_{BET}$ ($m^2/g$) | $V_p$ ($cm^3/g$) | $^aD_p$ (nm) | $^bS_{BET}$ ($m^2/g$) | $S_{BET}/\ ^bS_{BET}$ |
|---|---|---|---|---|---|
| SBA-15 | 818 | 1.05 | 5.78 | - | - |
| Ti(3)-SBA-15 | 581 | 0.55 | 4.93 | 793 | 0.73 |
| Ti(5)-SBA-15 | 693 | 0.83 | 5.25 | 777 | 0.89 |
| Ti(10)-SBA-15 | 628 | 0.77 | 5.27 | 736 | 0.85 |
| Ti(20)-SBA-15 | 498 | 0.52 | 4.18 | 654 | 0.76 |

[a]from BJH plot, desorption branch data, [b]Theoretical value considering well-dispersed non-porous $TiO_2$ phase component

Table 2. Textural properties of Pt supported on SBA-15 and on variousTi-SBA-15 materials prepared.

| Sample | $S_{BET}$ ($m^2/g$) | $V_p$ ($cm^3/g$) | [a]$D_p$ (nm) | [b]$S_{BET}$ ($m^2/g$) | $S_{BET}$/ [b]$S_{BET}$ |
|---|---|---|---|---|---|
| Pt(1.0)/SBA-15 | 609 | 0.68 | 4.82 | 810 | 0.75 |
| Pt(1.5)/SBA-15 | 663 | 0.84 | 5.4 | 806 | 0.82 |
| Pt(1.0)/Ti(10)-SBA-15 | 564 | 0.49 | 3.95 | 622 | 0.91 |
| Pt(1.5)/Ti(10)-SBA-15 | 612 | 0.54 | 3.87 | 619 | 0.99 |

[a]from BJH plot, desorption branch data, [b]Theoretical value considering well-dispersed non-porous $TiO_2$ phase component

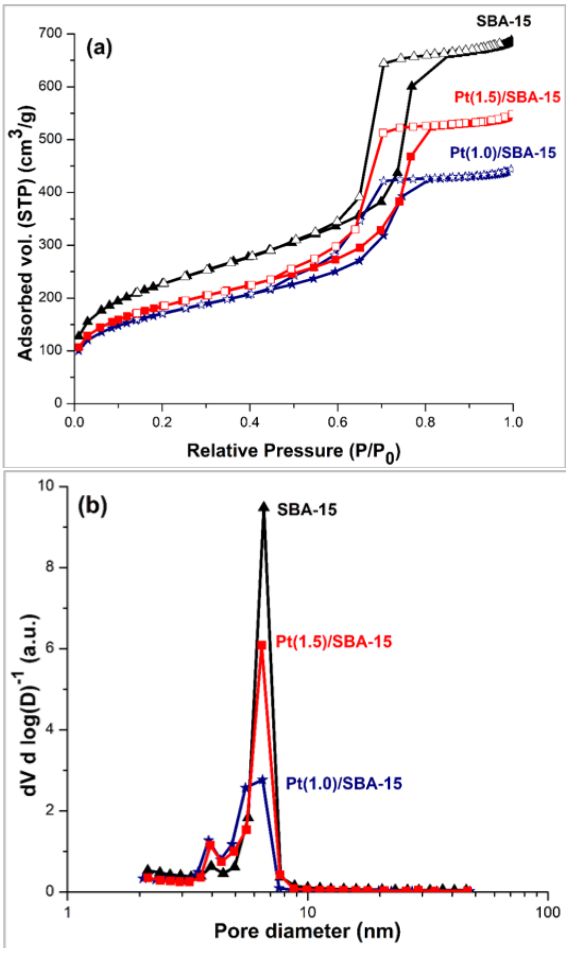


Fig. 2. (a) $N_2$ adsorption isotherms (at -198 °C) of Pt(1.0 and 1.5 wt%)/SBA-15 solids. Pristine support also included as reference. Open symbols: desorption branch; (b) Pore size distribution (BJH) of studied solids.

Accordingly, pore size distributions profiles (Figure 2(b)) showed contributions from smaller pores (~3.89 nm) as to those of non-impregnated siliceous carrier that could be rationalized by considering presence of some Pt crystals inside the carrier porous network.

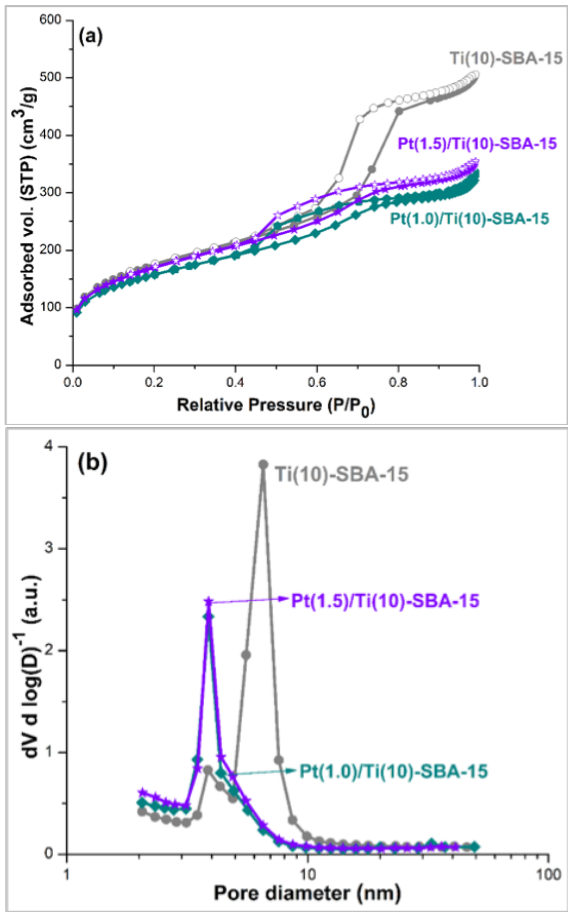


Fig. 3. (a) $N_2$ adsorption isotherms (at -198 °C) of SBA-15 modified with 10 wt% $TiO_2$ and corresponding Pt impregnated (1.0 and 1.5 wt%) solids. Open symbols: desorption branch; (b) Pore size distribution (BJH) of studied solids.

Positive effect of Ti-addition on Pt dispersion was evidenced by significantly diminished surface area loss (~6%, Table 2) for Pt(y)/Ti(10)-SBA-15 (y=1.0 or 1.5 wt%). Accordingly, very defined shift of PSD to lower diameters (see hysthereses loop closing in isotherms shifted to lower $P/P_o$ values and corresponding pore size profiles, Figure 3(a) and

(b), respectively) strongly suggested existence of Pt crystals inside Ti-modified SBA-15 pores. Taking into account the very limited $S_{BET}$ loss of Pt supported on Ti(10)-SBA.15 samples (column 6, Table 2), significantly high dispersion of deposited noble metal particles could be envisaged in those cases.

## *3.2 X-ray difracction*

A wide signal identified in the 15-35° 2$\theta$ range observed in diffractograms of all studied samples corresponded to amorphous silica constituting SBA-15 walls (Palcheva *et al*., 2016; Kolev *et al*., 2014), Figure 4. Reflexions at 25, 38, 48, 54, 55 and 62° corresponded to (101), (004), (200), (105), (211) and (204) planes of anatase titania phase (JCPDS 21-1272) (Tomer *et al*., 2015). Intensity of those signals increased with $TiO_2$ content pointing out to progressive crystal size growing (Calzada *et al*., 2019). Pt impregnated solids showed three main reflections at 2$\theta$ values of 39.8, 46.1 and 67.8° assigned to interplanar distances of (111), (200) and (220) face-centered cubic metallic platinum facets (PDF 01-087-0640), Figure 5(a). Unexpectedly, no supported $PtO_x$ species were found. In the opposite, metallic $Pt^0$ was evidenced.

Finding reduced platinum in calcined samples (see section *2.1.2 Pt impregnation*) supported on SBA-15 has been reported (as determined by XPS analysis) in the past by others (Ballesteros-Plata *et al*., 2019; Kolev *et al*., 2014) even though no explanation was advanced in those cases.

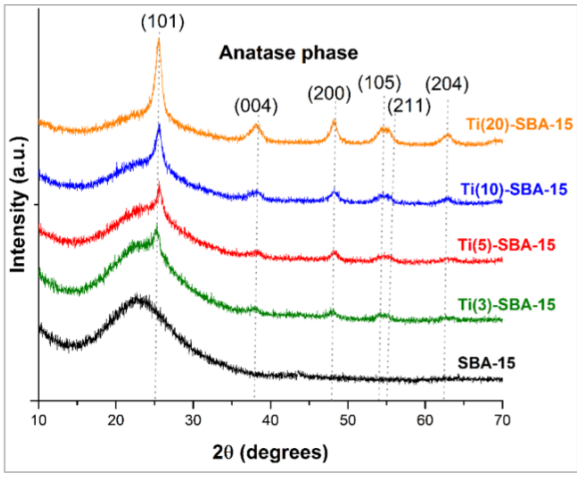


Fig. 4. Wide-angle X-ray diffraction patterns of SBA-15 and corresponding Ti-modified solids at various titanium contents.

We considered that organic remains that could be present on our mixed materials could play a determining role on that fact. Indeed, organic residua from Ti and Si alkoxides used during SBA-15 and corresponding Ti-modified solids synthesis usually could remain occluded in calcined materials (Escobar *et al*., 2000; Devi *et al*., 2018). Those organic species could contribute to Pt reduction during high-temperature annealing. Indeed, organic compounds had been sucessfully applied by others as noble metals reductants (Shiraishi *et al*., 2017). Also, glycols has been used to reduce platinum salts (Herricks *et al*., 2004) although differently to our case those organics were purportedly added.

According to Scherrer formula and by using the most intense Pt (111) reflection corresponding crystal size for solids with SBA-15 as carrier were estimated.

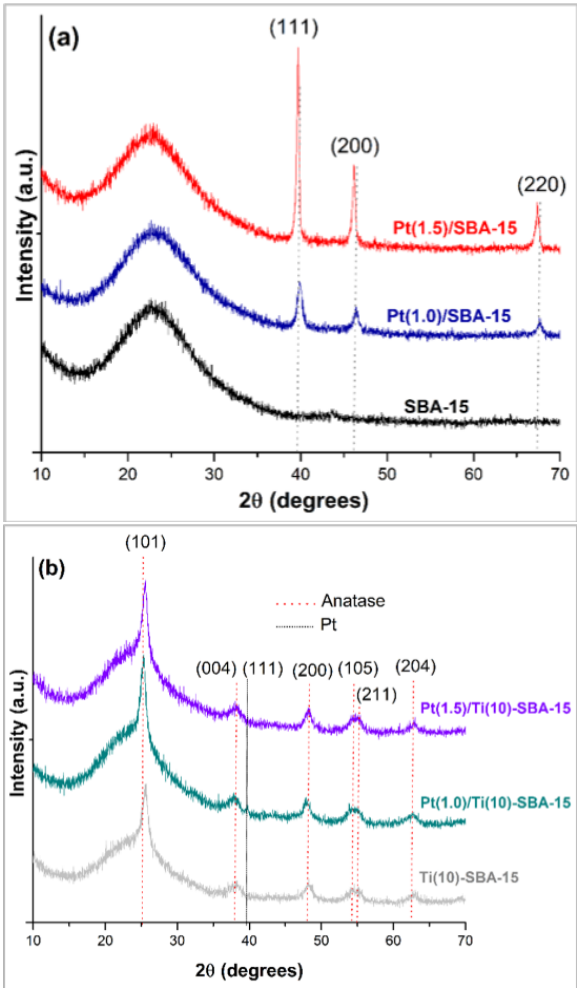


Fig. 5. Wide-angle X-ray diffraction patterns: (a) Pt-impregnated SBA-15; (b) Pt-impregnated Ti-modified solids at various platinum contents.

Platinum crystal size on pristine siliceous support increased two-fold (from 10 to 22 nm) by augmenting noble metal loading from 1 to 1.5 wt%. Others have reported (Kim *et al*., 2009) similar results to the latter when studying samples with 4 wt% platinum attributing that to low interaction of deposited species with silanol groups on silica surface. Due to that, in addition to low Pt dispersion after impregnation significant metallic particles sintering during high-temperature annealing could take place. Also, low noble metal dispersion could justifiy significant $S_{BET}$ loss of SBA-15-supported samples, much larger to those expected considering noble metal loading (see column 6 of Table 2). In these cases, Pt crystals dimensions were clearly big enough to plug some pores ($D_p$~5.8 nm, Table 1) of the pristine siliceous carrier.

Ti addition in SBA-15 matrix strongly promoted Pt dispersion as observed in Figure 5(b). Essentially undiscenarble Pt reflections on those materials precluded crystal size estimation although very small particle size beyond XRD detection limit (~3 nm) was evidenced by very tiny signals. The interaction between platinum and titania domains incorporated onto the siliceous support provided high Pt dispersion and deposited particles stability against sintering as well (Kim *et al*., 2009). It is worth noting that Ti incorporation method in carriers could also play a decisive role on Pt dispersion. Although presence of metallic platinum from $H_2PtCl_6$ thermal decomposition (500 °C) under air has been reported in the past in the case of silica-supported materials (Yamamoto *et al*., 2015) we consider that organic remains decomposition could also contribute to produce reduced noble metal nanoparticles. It seemed that those organic residua could accelerate impregnated platinum reduction during annealing conditions (500 °C) under air. Thus, reduction step under $H_2$ flow at 300-400 °C) (Li *et al*., 2017; Zhu *et al*., 2013) could be avoided simplifying then the catalyst activation procedure.

### *3.3 FTIR*

Broad bands centered around 3458 and 1634 1/cm were attributed to stretching vibrations of surface hydroxyl groups and water (Wang *et al*., 2007) and to deformation vibration of adsorbed un-dissociated $H_2O$ molecules coordinated to surface centers (Morterra, 1988), Figure 6. Shoulder at 3685 1/cm in all spectra could be related to surface silanol groups (Griffith, 1984).

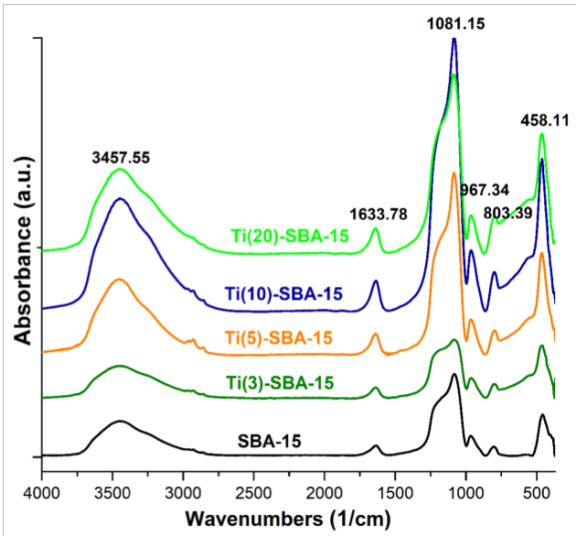


Fig. 6. FTIR spectra of pristine SBA-15 and various Ti-modified supports prepared.

Absorptions at 2970 and 2857 1/cm related to $-CH_3$ degenerated stretching mode and $-CH_2$ stretching symmetrical vibrations, respectively, indicated organic remans from Ti and Si alkoxides used during support synthesis (Escobar *et al*., 2017). As mentioned in previous section (3.2. *X-ray difracction*) those organic remains could contribute in reducing deposited platinum species supported on the prepared composites. Peak at around 1081 1/cm corresponded to Si-O-Si asymmetric stretching vibration meanwhile bands at ~803 and 458 1/cm were originated by symmetric stretching and deformation modes of aforementioned bonds. Although band at 967 1/cm could be typically considered as provoked by Si-O-Ti linkages in Ti-modified solids (Sahu *et al*., 2009) it could also contain contributions from Si-OH stretching vibrations (Wang *et al*., 2007). Thus, no unambiguous assignment could be carried out. Absence of surface defined crystalline titania domains could be stablished as corresponding Ti-O-Ti strechting bond at around 710 1/cm (Sahu *et al*., 2009) was not identified in studied spectra. Thus, most of anatase phase evidenced in X-ray diffractograms of Figure 4 and 5(b) could probably be encapsulated in the siliceous matrix due to very different sol-gel reactions (hydrolysis-condensation) rates of alkoxides used during synthesis (Escobar *et al*., 2000). Consequently, highly reactive Ti butoxide could generate titanium hydroxides domains before TEOS hydrolysis. Finally, band at 458 1/cm in studied spectra could be related to Si-O-Si bending vibrations (Azimov *et al*., 2012).

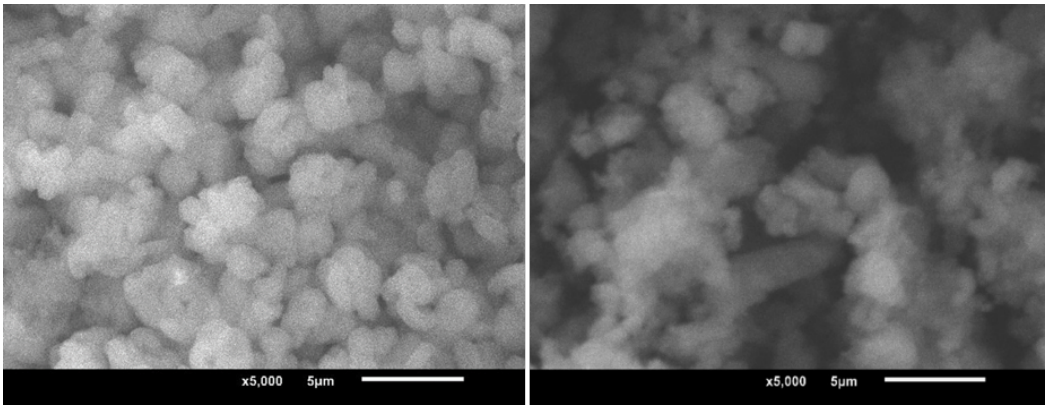


Fig. 7. SEM micrographs, 5000×, scale bar: 5 $\mu$m. (a) pristine SBA-15; (b) corresponding composite with 20 wt% $TiO_2$.

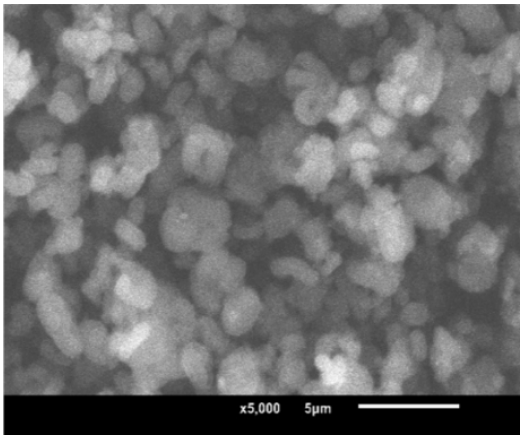


Fig. 8. SEM micrographs, 5000×, scale bar: 5 $\mu$m of Pt(1.0)/SBA-15.

### *3.4 Scannig electron microscopy (SEM)*

SBA-15 morphology exhibited particles of around 3-4 $\mu$m in diameter formed by numerous agglomerated hexagonal platelets of 800-1000 nm, Figure 7(a). Smooth platelets of very short length in axial direction were evidenced. In full agreement, others (Qin *et al*., 2013) identified alike morphology for SBA-15 prepared under similar conditions as to those used in the present investigation. To assess the influence of titanium addition on the siliceous material particles morphology the sample with the highest Ti content (20 wt% as $TiO_2$) was also analyzed, Figure 7(b). No significant differences on morphology as to that of pristine SBA-15 was observed although agglomerates dimensions seemed to be slightly enhanced on Ti-containing material. Probably that effect could be related to the characteristic high surface energy of titania anatase (identified by XRD, Figure 4) that renders that $TiO_2$ phase very prone to sintering under high-temperature annealing (Escobar *et al*., 2000). In full agreement with our findings no important effect of titanium on SBA-15 particles morphology has been found by others (Hung *et al*., 2013) although in that case cylinder-like aggregates comprised of so-called wheat grain shaped particles constituted pristine SBA-15. Also, Sn addition (in the 0.5-2 wt% range) did not significantly altered morphology of SBA-15 material consisting of rope-like domains of uniform size (~1 $\mu$m) (Li *et al*., 2017). Thus, although distinctive SBA-15 particles morphology seemed to depend upon specific synthesis conditions used in a given case it was also clear that modifiers (Ti, Sn, etc.) addition did not seriously affect it. After platinum impregnation on SBA-15, no appreciable morphological modifications as to that of pristine siliceous matrix were observed, Figure 8.

### *3.5 High-resolution TEM (HR-TEM) and high angle annular dark field-STEM (HAADF-STEM)*

The highly ordered honeycomb-shaped mesoporous structure of siliceous pristine SBA-15 containing hexagonal cross sections with pores of around 6 nm (Table 1) was evidenced in Figure 9(a). Also, well-ordered structure constituted by uniform channels along to pores axes was clearly observed, Figure 9(b). Those properties characteristic of 2-D hexagonal symmetry (*p6mm*) were in full agreement with corresponding structural characterization of SBA-15 materials as presented in previous works (Guo *et al*., 2017; Zhu *et al*., 2013; Azimov *et al*., 2012).

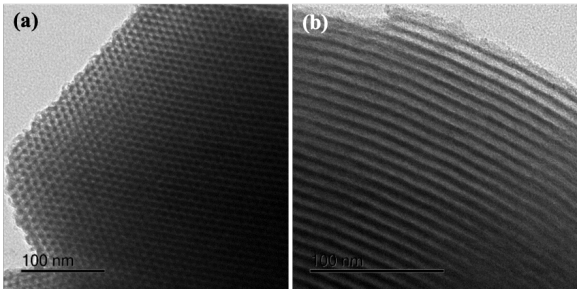


Fig. 9. HR-TEM micrographs of SBA-15 prepared: (a) Along pore axis direction; (b) Perpendicular to pore axis direction.

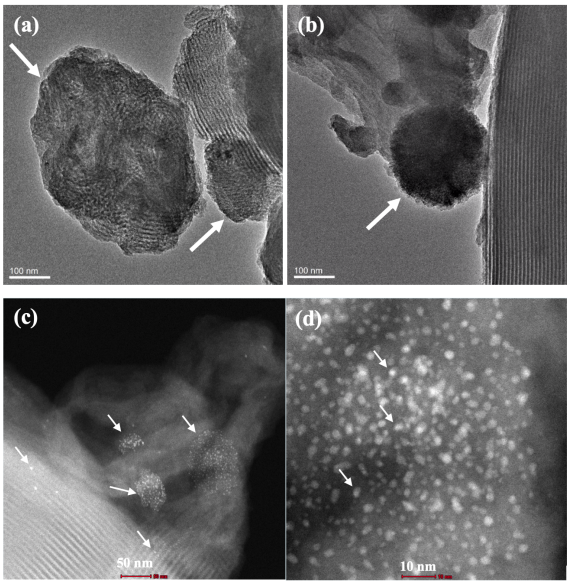


Fig. 10. (a) and (b) HR-TEM micrographs of Pt(1.5)/Ti(3)-SBA-15 material prepared; (c) and (d) corresponding HAADF micrographs. Large arrow: Anatase domains. Small arrows: Platinum crystals.

Regarding SBA-15 solids at various titania concentrations rounded titania anatase particles were observed, some of them segregated from SBA-15 (see for instance, Figure 10(b) and 12(b)) meanwhile others were clearly embedded in the ordered siliceous matrices (see Figure 10(a), 11(a)-(b) and 12(a)). In all materials both ordered parallel channels (SBA-15, very well preserved in the material of the lowest titania content, Figure 10(b)) and disordered mesoporous domains (related to $TiO_2$ phases) were evidenced. Those results suggested that titania phases could be incorporated within the siliceous mesostructured network (Yang *et al*., 2009). In the opposite to TEOS titanium butoxide could react vigorously with water producing metal hydroxides or hydrated oxides. During hydrolytic condensation an inorganic network is formed by a chain of hydrolysis and polymerization reactions (Yoldas, 1986). Thus, at the conditions use during synthesis of our mixed materials (see section *2.1.1 Ti-modified SBA-15*) titanium hydroxide domains could be formed before TEOS (of much lower reactivity, Boonstra and Baken, 1990) complete hydrolysis provoking presence of observed embedded anatase domains in the annealed binary materials. Others (Kolev *et al*., 2014) also reported rapid precipitation of titanium hydroxide (from Ti isopropoxide) in the low pH aqueous medium during SBA-15 synthesis from TEOS. In our case, $HNO_3$ could be an effective titanium butoxide hydrolysis catalyst (Escobar *et al*., 2000) enhacing then Ti hydroxides formation.

To get a better insigth on the Pt dispersion state over various mixed carriers prepared studied samples were analyzed by high-angle annular dark-field STEM (HAADF-STEM) in which the contrast in corresponding micrographs could be related to electrons scattered within the angular range characteristic of Rutherford scattering. In this technique, a finely focused probe of high energy electrons from scanning transmission electron microscope (STEM) is scanned across a thin sample to be analyzed. Although most of the beam could be diffracted at small angles some could be scattered through much larger ones, this component being collected by an annular detector and used to form the so-called Z-contrast image. As the cross-section for this type of scattering depends upon the square of the atomic number (Z) of analyzed atoms (i.e., $Z^2$), corresponding micrographs could enable chemical composition profiling based on image contrast (Hungría *et al*., 2019). Thus, in HAADF-STEM images heavier atoms (i.e., Pt ones) appear brighter than lighter ones (as those of Ti or Si).

Determination of structural characteristics (size, stacking and morphology) and location of $MoS_2$ phase on SBA-15 mesoporous matrix by HAADF-STEM has been reported (Girleanu *et al*., 2015). Also, that technique has been applied in the past to study dispersion of Pt impregnated on SBA-15 samples (Pinto *et al*., 2015).

In our case, it was clear that Pt particles were preferably deposited on titania domains although some platinum crystals inside mesoporous SBA-15 component where also evidenced (Figure 10(c)). Extremely small noble metal particles (~2 nm) were found over $TiO_2$ domains (Figure 10(d), 11(c) and 12 (c)) in full agreement with that found by XRD

(Figure 5(b)) where those tiny crystals could not be detected. However, large cubic platinum crystals were also found (Figures 11(d) and 12(d)) on samples supported on Ti-containing SBA-15 carriers.

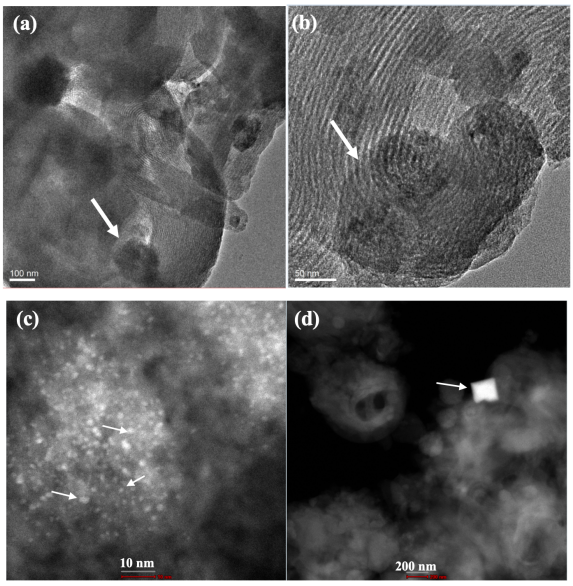


Fig. 11. (a) and (b) HR-TEM micrographs of Pt(1.0)/Ti(5)-SBA-15 material prepared; (c) and (d) corresponding HAADF micrographs. Large arrow: Anatase domains. Small arrows: Platinum crystals.

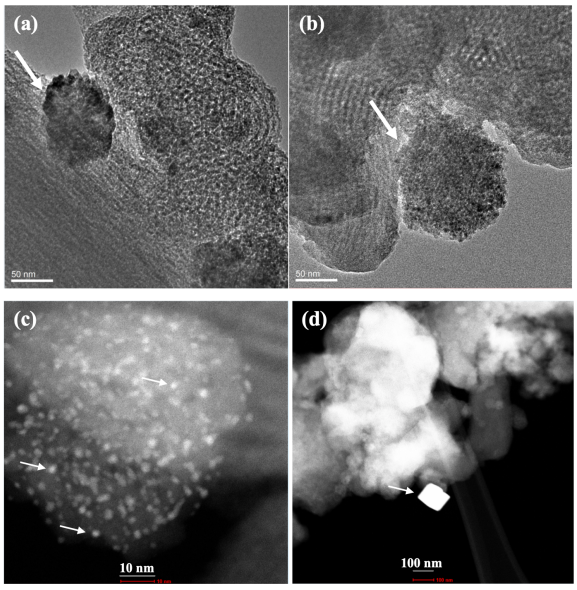


Fig. 12. (a) and (b) HR-TEM micrographs of Pt(1.0)/Ti(10)-SBA-15 material prepared; (c) and (d) corresponding HAADF micrographs. Large arrow: Anatase domains. Small arrows: Platinum crystals.

Those particles could result from sintering (particle migration-coalescence (Liu *et al.*, 2017)) under annealing at 500 °C (see section *2.1.2 Pt impregnation*) of noble metal particles originally deposited on the external siliceous carrier surface. They could be prone to sintering due to their weak interaction with the ordered $SiO_2$ surface, as reported by others (Liu *et al.*, 2017). Presence of those crystals large enough to partially plug some pores of binary supports could explain surface area lost of Pt(1.0)/Ti(10)-SBA-15 much bigger than expected considering noble metal loading (9% diminished $S_{BET}$, instead of 1% as that of $^{b}S_{BET}$, Table 2). It is worth mentioning that large Pt particles could be beneficial in catalytic activity depending on specific application. For instance, regarding Pt/ceria-zirconia formulations tested in the ethanol and toluene oxidation (Topka *et al.*, 2016) superior performance was observed for materials at 0.59 and 1 wt% Pt that being ascribed to large noble metal nanoparticles (36 and 45 nm, as determined by HR-TEM). Those nanocrystals were absent in materials of lower platinum loading where smaller ones (3 nm) were identified. One interesting point that remains to be elucidated consists in the reducing effect (on deposited Pt species) of organic residua from alkoxides decomposition during high-temperature annealing of noble metal impregnated composites. Whether that phenomenon could also influence $TiO_2$ phases resulting in their partial reduction (then in SMSI, Strong Metal Support Interaction Effect (Escobar *et al.*, 2002; Escobar *et al.*, 2006)) it is undoubtedly a topic worth investigating.

The beneficial effect of titania on platinum dispersion in prepared SBA-15-based composites was clearly demonstrated in this work. Expectedly, that improvement could be reflected in enhanced catalytic activity. Obtained materials will be tested in reactions of hydrodeoxygenation of biomass-derived species. Those investigations are in due course and will be the subject of upcomig reports.

## Conclusions

Pt (1 and 1.5 wt%) was impregnated by incipient wetness on Ti-modified SBA-15 composites at different $TiO_2$ contents (3, 5, 10 and 20 wt%). Pristine SBA-15 had surface area greater than 800 $m^2/g$ that progressively decreased with increasing $TiO_2$ content in composites. Very different hydrolysis

rate of titanium butoxide and tetraethyl orthosilicate alkoxides used during synthesis could provoke encapsulation of some segregated titania domains in the SBA-15 structure. Highly reactive titanium butoxide hydrolysis-condensation could take place before those reactions corresponding to tetraethyl orthosilicate. Pt dispersion clearly augmented with Ti concentration in composites. Corresponding pore size profiles maxima clearly shifted to lower diameters (as to that of non-impregnated supports) after platinum loading suggesting location of noble metal crystals inside the pores of SBA-15 and titania-modified siliceous carriers, that effect being much clearer in the latter. However, some large cubic platinum crystals were also observed probably due to sintering (during calcining at 500 °C) of Pt particles weakly interacting with the siliceous SBA-15 component. Interestingly, after materials annealing (500 °C under static air) metallic platinum was evidenced (by XRD) pointing out to noble metal reduction by decomposition of organic remains from alkoxides used during carriers synthesis. Thus, reduction step during corresponding catalyst synthesis could be avoided.

### *Acknowledgements*

G. Morales Hernández acknowledges UJAT-DACB and IMP for their support on carrying out the present investigation. She is also is grateful to CONACYT (Mexico) by Master in Science scholarship provided (639500).

## References

Araujo, M.M. Silva, L.K.R., Sczancoski, J.C., Orlandi, M.O., Longo, E., Santos, A.G.D., Sá, J.L.S., Santos, R.S., Luz Jr. G.E. and Cavalcante, L.S. (2016). Anatase $TiO_2$ nanocrystals anchored at inside of SBA-15 mesopores and their optical behavior. *Applied Surface Science 389*, 1137-1147. https://doi.org/10.1016/j.apsusc.2016.08.018

Azimov, F., Markova, I., Stefanova, V. and Sharipov, Kh. (2012). Synthesis and characterization of SBA-15 and Ti-SBA-15 nanoporous materials for DME catalysts. *Journal of the University of Chemical Technology and Metallurgy 47*, 333-340.

Ballesteros-Plata, D., Infantes-Molina, A. and Rodríguez-Castellón, E. (2019). Study of bifunctionality of Pt/SBA-15 catalysts for HDO of Dibenzofuran, reaction: Addition of Mo or use of an acidic support. *Applied Catalysis A-General 580*, 93-101. https://doi.org/10.1016/j.apcata.2019.05.002

Boonstra, A.H. and Baken, E. (1990). Relation between the acidity and reactivity of a TEOS, etanol and water mixture. *Journal of Non-Crystalline Solids 122*, 171-182. https://doi.org/10.1016/0022-3093(90)91063-W

Calzada, L.A., Castellanos, R., García, L.A. and Klimova, T.E. (2019). $TiO_2$, $SnO_2$ and ZnO catalysts supported on mesoporous SBA-15 versus unsupported nanopowders in photocatalytic degradation of methylene blue. *Microporous and Mesoporous Materials 285*, 247-258. https://doi.org/10.1016/j.micromeso.2019.05.015

Cui, X., Wang J., Zhang X., Wang, Q., Song, M. and Chai, J. (2019). Preparation of nano-$TiO_2$ by a surfactant-free microemulsion-hydrothermal method and its photocatalytic activity. *Langmuir 35*, 9255-9263. doi: 10.1021/acs.langmuir.9b01392

Devi, P., Das, U. and Dalai, A.K. (2018). Production of glycerol carbonate using a novel Ti-SBA-15 catalyst. *Chemical Engineering Journal 346*, 477-488. https://doi.org/10.1016/j.cej.2018.04.030

Escobar, J., De los Reyes, J.A. and Viveros, T. (2000). Influence of the synthesis additive on the textural and structural characteristics of sol-gel $Al_2O_3$-$TiO_2$. *Industrial Engineering Chemistry Research 39*, 666-672. https://doi.org/10.1021/ie990487o

Escobar, J., De los Reyes, J.A. and Viveros, T. (2002). Nickel on $TiO_2$-modified $Al_2O_3$ sol-gel oxides: Effect of synthesis parameters on the supported phase properties. *Applied Catalysis A-Gen 253*, 151-163. doi:10.1016/S0926-860X(03)00501-5

Escobar, J., De Los Reyes, J.A., Viveros, T. and Barrera, M.C. (2006). Cyclohexane dehydrogenation over wet-impregnated Ni on $Al_2O_3$-$TiO_2$ sol-gel oxides. *Industrial*

*Engineering Chemistry Research 45*, 5693-5700. https://doi.org/10.1021/ie050844x

Escobar, J., Barrera, M.C., Gutiérrez, A.W. and Terrazas, J.E. (2017). Benzothiophene hydrodesulfurization over NiMo/alumina catalysts modified by citric acid. Effect of addition stage of organic modifier. *Fuel Processing Technology 156* 33-42. https://doi.org/10.1016/j.fuproc.2016.09.028

Flodström, K. and Alfredsson, V. (2003). Influence of the block length of triblock copolymers on the formation of mesoporous silica. *Microporous and Mesoporous Materials 59*, 167-176. https://doi.org/10.1016/S1387-1811(03)00308-1

Girleanu, M., Lopes Silva, S., Ihiawakrim, D., Chaumonnot, A., Bonduelle-Skrzypczak, A., Lefebvre, F., Dufaud, V., Gay, A-S. and Ersen, O. (2015). HAADF-STEM high-resolution study of nanometric $MoS_2$ inside mesoporous SBA-15. *Microporous and Mesoporous Materials 217*, 190-195. DOI:10.1016/j.micromeso.2015.06.021

Gómez-Orozco, S.Y., Huirache-Acuña, R., Pawelec, B., Fierro, J.L.G., Rivera-Muñoz, E.M., Lara Romero, J. and Alonso Nuñez, G. (2018). Characterizations and HDS performances of sulfided NiMoW catalysts supported on mesoporous titania-modified SBA-15. *Catalysis Today 305*, 152-161. https://doi.org/10.1016/j.cattod.2017.08.009

Griffith, G.W. (1984). Quantitation of silanol in silicones by FTIR spectroscopy. *Industrial Engineering Chemistry Product Research Development 23*, 590-593. https://doi.org/10.1021/i300016a015

Guo, X., Feng, Y., Ma, L., Gao, D., Jing, J., Yu, J., Sun, H., Gong, H. and Zhang, Y. (2017). Phosphoryl functionalized mesoporous silica for uranium adsorption. *Applied Surface Science 402*, 53-60. https://doi.org/10.1016/j.apsusc.2017.01.050

Herricks, T., Chen, J. and Xia, Y. (2004). Polyol synthesis of platinum nanoparticles: control of morphology with sodium nitrate. *Nano Letters 4*, 2367-2371. https://doi.org/10.1021/nl048570a

Hung, N.P., Hoan, N.T.V. and Nghia, N.V. (2013). Synthesis and characterization of photocatalytic material $TiO_2$/SBA-15. *Nanoscience and Nanotechnology 3*, 19-25. DOI: 10.5923/j.nn.20130301.04

Hungría, A.B., Calvino, J.J., Hernández-Garrido, J.C. (2019). HAADF STEM Electron tomography in catalysis research A. *Topics in Catalysis 62*, 808-821. https://doi.org/10.1007/s11244-019-01200-2

Iglesias, J., Melero, J.A. and Sainz-Pardo, J. (2008). Direct synthesis of organically modified Ti-SBA-15 materials. *Journal of Molecular Catalysis A-Chemical 291*, 75-84. https://doi.org/10.1016/j.molcata.2008.06.004

Kim, M.Y., Jung, S.B., Kim, M.G., You, Y.S., Park, J.-H., Shin, C.-H. and Seo, G. (2009). Preparation of highly dispersive and stable platinum catalysts supported on siliceous sba-15 mesoporous material: roles of titania layer incorporation and hydrogen peroxide treatment. *Catalysis Letters 129*, 194-206. DOI: 10.1007/s10562-008-9790-0

Kolev, H., Todorova, S., Naydenov, A., Ene, R., Ivanov, G., Parvulescu, V. and Kadinov, G. (2014). Catalytic activity of mesoporous SBA-15 modified with Pt and Ti in a deep methane, n-hexane and CO oxidation. *Athens Journal of Sciences 1*, 9-20. https://doi.org/10.30958/ajs.1-1-1

Kumar, M.S., Chen, D., Walmsley, J.C. and Holmen, A. (2008). Dehydrogenation of propane over Pt-SBA-15: Effect of Pt particle size. *Catalysis Communications 9*, 747-750. https://doi.org/10.1016/j.catcom.2007.08.015

Leofanti, S.G., Padovan, M., Tozzola, G., Venturelli, B. (1998). Surface area and pore texture of catalysts. *Catalysis Today 41*, 207-210. doi:10.1016/S0920-5861(98)00050-9

Li, B., Xu, Z., Chu, W., Luo, S. and Jing, F. (2017). Ordered mesoporous Sn-SBA-15 as support for Pt catalyst with enhanced performance in propane dehydrogenation. *Chinese Journal of Catalysis 38*, 726-735. DOI: 10.1016/S1872-2067(17)62805-5

Liu, J., Ji, Q., Imai, T., Ariga, K. and Abeb, H. (2017). Sintering-resistant nanoparticles in wide-mouthed compartments for sustained catalytic performance. *Scientific Reports 7*, 1-8. DOI: 10.1038/srep41773

Morterra, C. (1988). An infrared spectroscopic study of anatase properties. Part 6. -Surface hydration and strong Lewis acidity of pure and sulphate-doped preparations. *Journal of the Chemical Society, Faraday Transactions 1*, 1617-1637. DOI:10.1039/F19888401617

Palcheva, R., Kaluža, L., Dimitrov, L., Tyuliev, G., Avdeev, G., Jirátová, K. and Spojakina, A. (2016). NiMo catalysts supported on the Nb modified mesoporous SBA-15 and HMS: effect of thioglycolic acid addition on HDS. *Applied Catalysis A-General 520*, 24-34. https://doi.org/10.1016/j.apcata.2016.04.008

Pinto, T., Arquillière, P., Niccolai, G.P., Lefebvre, F. and Dufaud, V. (2015). The comparison of two classes of bifunctional SBA-15 supported platinum-heteropolyacid catalysts for the isomerization of n-hexane. *New Journal of Chemistry 39*, 5300-5308. DOI: 10.1039/c5nj00453e

Qin, Y., Wang, Y., Wang, H., Gao, J. and Qu, Z. (2013). Effect of morphology and pore structure of SBA-15 on toluene dynamic adsorption/desorption performance. *Procedia Environmental Sciences 18*, 366-371. https://doi.org/10.1016/j.proenv.2013.04.048

Sahu, D.R., Hong, L.Y., Wang, S.C. and Huang, J.L. (2009). Synthesis, analysis and characterization of ordered mesoporous $TiO_2$/SBA-15 matrix: Effect of calcination temperature. *Microporous and Mesoporous Materials 117*, 640-649. https://doi.org/10.1016/j.micromeso.2008.08.013

Schwanke, A.J., Favero, C., Balzer, R., Bernardo-Gusmão, K. and Pergher, S.B.C. (2018). SBA-15 as a support for nickel-based catalysts for polymerization reactions. *Journal of Brazilian Chemical Society 29*, 328-333. http://dx.doi.org/10.21577/0103-5053.20170144

Sharma R.V., Baroi, Ch. and Dalai, A.K. (2014). Production of biodiesel from unrefined canola oil using mesoporous sulfated Ti-SBA-15 catalyst. *Catalysis Today 237*, 3-12. https://doi.org/10.1016/j.cattod.2014.07.005

Shiraishi, Y., Tanaka, H., Sakamoto, H., Ichikawa, S. and Hirai, T. (2017). Photoreductive synthesis of monodispersed Au nanoparticles with citric acid as reductant and surface stabilizing reagent. *RSC Advances 7*, 6187-6192. DOI: 10.1039/C6RA27771C

Sing, K.S.W., Everett, D.H., Haul, R.A.W., Moscou, L., Pierotti, R.A., Rouquérol, J. and Siemieniewska, T. (1985). Reporting physisorption data for gas/solid systems. *Pure Applied Chemistry 57*, 603-619. http://dx.doi.org/10.1351/pac198557040603

Singh, S., Kumar, R., Setiabudi, H.D. and Nanda, S. (2018). Advanced synthesis strategies of mesoporous SBA-15 supported catalysts for catalytic reforming applications: A state-of-the-art review. *Applied Catalysis A-General 559*, 57-74. https://doi.org/10.1016/j.apcata.2018.04.015

Tomer, V.K., Jangra, S., Malik, R. and Duhan, S. (2015). Effect of *in-situ* loading of nano titania particles on structural ordering of mesoporous SBA-15 framework. *Colloids and Surfaces A: Physicochemical and Engineering Aspects 466*, 160-165. https://doi.org/10.1016/j.colsurfa.2014.11.025

Topka, P., Kaluža, L. and Gaálová, J. (2016). Total oxidation of ethanol and toluene over ceria-zirconia supported platinum catalysts. *Chemical Papers 70*, 898-906. https://doi.org/10.1515/chempap-2016-0028

Torres-Santillán, E., Vargas-García, J.R., Ramírez-Meneses, E., Manzo-Robledo, A. and Hernández-Pérez, M.A. (2019). Induced electrochemical reduction of nitrates species on inteface of Pt/MWCNTs prepared by vapor-phase impregnation decomposition method. *Revista Mexicana de Ingeniería Química 18*, 431-439. https://doi.org/10.24275/uam/izt/dcbi/revmexingquim/2019v18n2/Torres

Wang, Z., Zhang, F., Yang, Y., Xue, B., Cui, J. and Guan, N. (2007). Facile postsynthesis of visible-light-sensitive titanium dioxide/mesoporous SBA-15. *Chemistry of Materials 19*, 3286-3293. https://doi.org/10.1021/cm062041l

Wu, H. C., Chen, T.C., Lai N.C., Yang, C.M., Wu, Y.H., Chen, Y.C., Lee, J.F. and Chen, C.S. (2015). Synthesis of sub-nanosized Pt particles on mesoporous SBA-15 material and its application to the CO oxidation reaction. *Nanoscale 7*, 16848-16859. DOI: 10.1039/C5NR04943A

Yamamoto, T., Miyamoto, K., Kondo, M. and Yukumoto, A. (2015). Analysis of d-electron state of platinum salts on silica during thermal decomposition by a laboratory-type X-ray absorption spectrometer - choice of parameters for *in situ* experiments. *Bunseki kagaku 64*, 889-894. DOI:10.2116/bunsekikagaku.64.889

Yang, H.C., Lin, H.Y., Chien, Y.S., Chi-Sheng, J., Wu, J. C.-S. and Wu, H.H. (2009). Mesoporous $TiO_2$/SBA-15, and Cu/$TiO_2$/SBA-15 composite photocatalysts for photoreduction of $CO_2$ to methanol. *Catalysis Letters 131*, 381-387. DOI 10.1007/s10562-009-0076-y

Yin, Y., Yang, Z.F., Wen, Z.H., Yuan, A.H., Liu, X.Q., Zhang, Z.Z. and Zhou, H. (2017). Modification of as synthesized SBA-15 with Pt nanoparticles: Nanoconfinement effects give a boost for hydrogen storage at room temperature. *Scientific Reports 7*, 1-10. https://doi.org/10.1038/s41598-017-04346-9

Yoldas, B.E. (1986). Hydrolysis of titanium alkoxide and effects of hydrolytic polycondensation parameters. *Journal of Materials 21*, 1087-1092. DOI: https://doi.org/10.1007/BF01117399

Zhang, P., Wu, H., Fan, M., Sun, W., Jiang, P. and Dong, Y. (2019). Direct and postsynthesis of Ti-incorporated SBA-15 functionalized with sulfonic acid for efficient biodiesel production. *Fuel 235*, 426-432. https://doi.org/10.1016/j.fuel.2018.08.029

Zhu, J., Wang, T. and Xu, X. (2013). Pt nanoparticles supported on SBA-15: Synthesis, characterization and applications in heterogeneous catalysis. *Applied Catalysis B- Environmental 130-131*, 197-217. http://dx.doi.org/10.1016/j.apcatb.2012.11.005.

Ziarani, G.M., Rohani, S., Ziarati, A. and Badiei, A. (2018). Applications of SBA-15 supported Pd metal catalysts as nanoreactors in C-C coupling reactions. *RSC Advances 8*, 41048-41100. DOI: 10.1039/c8ra09038f.